Low phonon conductivity of layered BiCuOS, BiCuOSe, and BiCuOTe from first principles

Hyo Seok Ji,[1] Atsushi Togo,[2] Massoud Kaviany,[3,4] Isao Tanaka,[2,5,6,7] and Ji Hoon Shim[1,4,8,*]

[1]*Department of Chemistry, Pohang University of Science and Technology, Pohang 790-784, Korea*
[2]*Center for Elements Strategy Initiative for Structure Materials (ESISM), Kyoto University, Sakyo, Kyoto 606-8501, Japan*
[3]*Department of Mechanical Engineering, University of Michigan, Ann Arbor, Michigan 48109-2125, USA*
[4]*Division of Advanced Nuclear Engineering, Pohang University of Science and Technology, Pohang 790-784, Korea*
[5]*Department of Materials Science and Engineering, Kyoto University, Sakyo, Kyoto 606-8501, Japan*
[6]*Center for Materials Research by Information Integration, National Institute for Materials Science, Tsukuba 305-0047, Japan*
[7]*Nanostructures Research Laboratory, Japan Fine Ceramics Center, Nagoya 456-8587, Japan*
[8]*Department of Physics, Pohang University of Science and Technology, Pohang 790-784, Korea*

(Received 29 April 2016; revised manuscript received 10 August 2016; published 14 September 2016)

Combining the effect of layer mixing, mass mismatch, and intrinsic defects, we have investigated the origin of very low phonon conductivity k_p in thermoelectric (TE) BiCuOQ (Q: S, Se, Te) compounds. Based on the first-principles anharmonic, lattice dynamics calculations, we use the single-mode relaxation time approximation of the linearized phonon Boltzmann equation, which shows good agreement with experiments. Here, we found that the most important parameter for low k_p is the interlayer interaction between the BiO and CuQ layers. By analyzing the phonon linewidth distribution, which indicates the phonon scattering rate, we propose that the interlayer interactions play a critical role on suppressing k_p, i.e., the heterolayered crystal controls these interlayer interactions, achieving low k_p and optimal TE properties.

DOI: 10.1103/PhysRevB.94.115203

I. INTRODUCTION

Lowering thermal conductivity is the most important issue in thermoelectric (TE) material development. TE efficiency is quantified by the figure of merit $ZT = S^2\sigma_e T/k$, where S, σ_e, T, and k are the Seebeck coefficient, electrical conductivity, absolute temperature, and thermal conductivity. So, efficient TE materials essentially need the low k in addition to the optimization of the power factor (PF) $S^2\sigma_e$. The total thermal conductivity $k = k_e + k_p$ consists of both electronic and phonon contributions. For semiconductors (most of TE materials), the phonon contribution usually surpasses the electronic contribution, so lowering k_p becomes important. Indeed, there has been much research on achieving low k_p, such as the phonon glass-electron crystal [1], the construction of rattling ions in crystal [2–6], nanostructuring [7–10], and all-scale hierarchical architecting [11]. From the phonon perspective, the mass mismatch of layers can lead to phonon scattering and low k_p. Indeed, the heterolayered BiCuOQ compounds (Q: chalcogen elements S, Se, and Te) have been reported to be good candidates for high ZT with intrinsically low k_p.

The p-type BiCuOSe (BiCuSeO or BiOCuSe) is a recently reported high-ZT thermoelectric (TE) material, i.e., $ZT = 1.4$ at 923 K [12]. The pristine compound exhibits intrinsically low k_p($<$1.0 W/m K), and its electrical conductivity is also small due to low hole mobility [13–16]. By doping with cations such as Ba^{2+} into the Bi^{3+} site, however, the electrical conductivity as well as its PF have significantly increased. Further enhancement of the PF through doping with light atoms increases both the carrier concentration and the mobility. Although its PF is smaller than other highly efficient TE materials, BiCuOSe can have high ZT values because of its very low k_p.

Figure 1(a) shows a typical BiCuOQ tetragonal crystal structure that is a ZrSiCuAs-type structure with a space group of $P4/nmm$. The unit cell consists of two different layers stacking along the c axis, which are the conducting $[Cu_2Q_2]^{2-}$ and insulating $[Bi_2O_2]^{2+}$ layers. It was reported that the mixing of two different layers allows the control of the electronic band gap, as well as the band structures around the band gap to induce the high PF [11]. The two different layers in this compound are intrinsically mixed with a simple synthesizing technique, and various types of doping in each layer are available. For BiCuOSe, the band gap is given by 0.8 eV with the valence band of $[Cu_2Se_2]^{2-}$ character and the conduction band of $[Bi_2O_2]^{2+}$ character, as illustrated in Fig. 1(b) [18,19].

The TE properties S and σ_e of the BiCuOQ compounds have been predicted by the Boltzmann transport equation (BTE) combined with the first-principles band-structure calculations. Using a simple rigid-band and the constant relaxation time approximation (RTA), the calculated PF showed good agreement with experimental results at the same doping condition. Moreover, the electronic structure calculations also suggested the optimal charge-carrier density doping maximizing the PF of BiCuOQ compounds [18] and verifying the origin of anomalous increases of hole-carrier concentration of Pb-doped BiCuOTe [20]. The k, however, cannot be described by the electronic structures only because the phonon contribution may dominate over the electronic contribution. So, accurate prediction of ZT in BiCuOQ compounds requires the prediction of k_p.

There are two common theoretical treatments of the phonon transport, namely, atomistic molecular dynamics (MD) technique and continuum transport theory. The MD simulations provides the insight into the lattice dynamics at the atomic level. With a given material structure and suitable interatomic potentials, the MD simulations have been used to match well the experimental lattice properties of simple two-atom TE materials [21,22]. However, the semiempirical interatomic

*Corresponding author: jhshim@postech.ac.kr

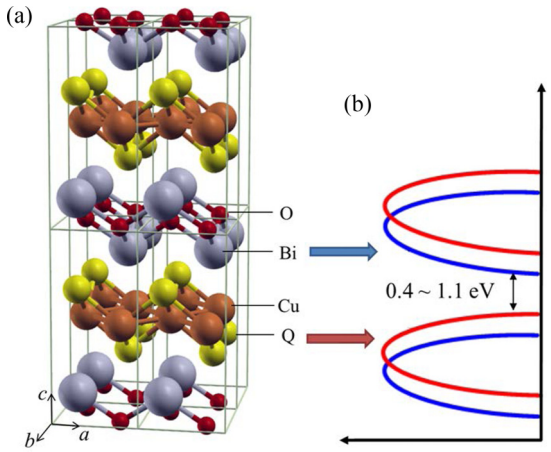

FIG. 1. (a) Atomic structure of the ZrSiCuAs-type BiCuOQ compound. (b) Schematic diagram illustrating the electronic density of states (DOS) of BiCuOQ based on the concept of mixed-layer systems [17].

potentials are generally obtained by fitting the experimental lattice properties. So the complex systems are very challenging to describe their atomic interactions with simple two-body and three-body interactions. To overcome this limitation, the *ab initio* MD simulations have been used for simple systems with advances in computing resources [23,24]. The advantage is no need for fitting to existing experimental data, but it is computationally extensive. Another approach is the continuum transport theory (or kinetic theory), such as the phonon BTE, which is suitable for fast calculation of large systems. Recent development of the perturbation theory within density functional theory (DFT) allows for the third-order force constant matrices to be determined without resorting to the numerical differentiation. This facilitates the investigation of accurate phonon dispersion, including anharmonicity [25]. Because the BTE requires only the phonon dispersion, the combination of the BTE and the first-principles phonon calculations have enabled the accurate prediction of phonon transport properties [26].

Recent investigations of k_p in BiCuOSe systems have used the combined approach of the first-principles and the lattice dynamics calculations [19,27]. Saha [19] has suggested the origin of low k_p by comparing the vibrational modes of BiCuOSe and LaCuOSe. The low k_p of BiCuOSe is ascribed to its heavy atomic mass of Bi and high anharmonicity indicated by the Grüneisen parameter. Shao *et al.* [27] also have investigated k_p of BiCuOSe by solving the phonon BTE with anharmonic force constants and also emphasized the anharmonicity as an origin of the low k_p. They also pointed out the anisotropy and the importance of the optical phonon in low k_p as a report. However, there have been few studies on the origin of high anharmonicity in this system, as well as its control, based on atomic doping or substitution. So, more systematic analysis in the anharmonic phonon calculation is needed to find the key factor for low k_p in heterolayered compounds.

Here, we investigate the k_p for the series of BiCuOQ compounds using a combined approach of the first-principles calculation and the phonon BTE under the RTA. For understanding the mechanism of low k_p, we also compare the phonon modal scattering rates of BiCuOQ compounds using many-body perturbation theory with the anharmonic force constants. Our results reproduce well the reported k_p and structural properties in experiments. Moreover, we show that the interlayer interaction has an important role to lower the k_p, based on the comparative analysis of the frequency-dependent scattering rate in three parent compounds BiCuOS, BiCuOSe, and BiCuOTe.

II. METHODS

A. *Ab initio* calculations

In the DFT calculations of BiCuOQ, we use the frozen-core projector augmented wave method [28,29] encoded in the Vienna *ab initio* simulation package [30], and the generalized-gradient approximation of Perdew-Burke-Ernzerhof prescription for solid (PBEsol) [31] for the exchange-correlation functional with the plane-wave–cut-off energy of 500 eV. The Brillouin zones of the tetragonal unit cells were sampled by $6 \times 6 \times 2$ k-point meshes generated in accordance with the Monkhorst-Pack scheme [32]. The $6s$,$6d$, and $6p$ electrons of Bi atom, the $3p$,$4s$, and $4d$ electrons of Cu atom, the $2s$ and $2p$ electrons of O atom, and the ns and np electrons for Q atom ($n = 3$ for S, 4 for Se, and 5 for Te) were treated as valence and the remaining electrons were kept frozen. To obtain atomic forces, the total energies were minimized until the energy convergences were less than 10^{-8} eV. The lattice parameters are then optimized under zero-pressure condition.

The second- and third-order force constants were obtained by the supercell approach [33,34] with finite atomic displacement of 0.03 Å. In the finite-difference calculations, we use $3 \times 3 \times 1$ supercells containing 72 atoms with 8 different atomic displacements for second-order and 1514 displacements for third-order force constants, while containing full nearest neighbors in the $3 \times 3 \times 1$ supercell. We have also verified the size effect on the phonon dispersion and k_p with $3 \times 3 \times 2$ and $4 \times 4 \times 1$ supercells by comparing with $3 \times 3 \times 1$ results. The reciprocal cells of the supercells were sampled by $2 \times 2 \times 2$ k-point meshes using the Monkhorst-Pack scheme.

B. Phonon conductivity and modal scattering rate

To calculate the phonon conductivity, the BTE is used within the RTA, which is implemented in the PHONO3PY package [26]. The phonon conductivity tensor is [35]

$$\mathbf{K}_p = \sum_{\lambda} C_\lambda \vec{v}_\lambda \otimes \vec{v}_\lambda \tau_\lambda, \tag{1}$$

where C_λ is the modal heat capacity, and $\vec{v}_\lambda$ and τ_λ are the group velocity and phonon relaxation time for phonon mode λ. Here the phonon modes, including the wave vector $\mathbf{q}$ and the band indices j ($\mathbf{q}$,j) and (-$\mathbf{q}$,j), have been abbreviated by λ and $-\lambda$, respectively.

The phonon relaxation time is calculated from the imaginary part of the self-energy considering up to three phonons participating in scattering using many-body perturbation theory. It takes the form analogous to the Fermi golden

TABLE I. Calculated lattice parameters, Born effective charges $z_{M,\alpha}$, and dielectric constants $\varepsilon_{\infty,\alpha}$ of BiCuOQ. The lattice constants in parentheses are experimental results [16].

Compound	a (Å)	c (Å)	$z_{Bi,\parallel}$	$z_{Bi,\perp}$	$z_{Cu,\parallel}$	$z_{Cu,\perp}$	$z_{O,\parallel}$	$z_{O,\perp}$	$z_{Q,\parallel}$	$z_{Q,\perp}$	$\varepsilon_{\infty,\parallel}$	$\varepsilon_{\infty,\perp}$
BiCuOS (this work)	3.84 (3.86)	8.46 (8.56)	5.87	5.77	1.02	0.61	−3.71	−4.03	−3.10	−2.35	12.70	11.45
BiCuOSe (this work)	3.89 (3.93)	8.89 (8.93)	6.27	5.85	1.15	1.08	−4.09	−4.30	−3.13	−2.64	14.25	13.90
BiCuOTe (this work)	3.99 (4.04)	9.51 (9.52)	6.50	6.38	0.97	1.24	−4.44	−4.89	−2.59	−2.73	15.80	17.11
BiCuOSe (PBE, [27])	3.96	9.12	6.51	6.05	1.52	1.14	−4.31	−4.42	−3.73	−2.76	18.64	14.01
BiCuOSe (PBEsol, [19])	3.90	8.92	6.46	5.93	1.44	1.06	−4.28	−4.42	−3.67	−2.70	18.01	13.79

rule [36],

$$\Gamma_\lambda(\omega) = \frac{18\pi}{\hbar^2}\sum_{\lambda'\lambda''}|\Phi_{-\lambda\lambda'\lambda''}|^2\{(f_{\lambda'}+f_{\lambda''}+1)\delta(\omega-\omega_{\lambda'}-\omega_{\lambda''}) + (f_{\lambda'}-f_{\lambda''})[\delta(\omega+\omega_{\lambda'}-\omega_{\lambda''}) - \delta(\omega-\omega_{\lambda'}+\omega_{\lambda''})]\}, \quad (2)$$

where f_λ is the phonon equilibrium occupancy and $\Phi_{\lambda\lambda'\lambda''}$ is the strength of interaction among the three phonons λ, λ', and λ'' involved in the scattering, which is explicitly given by Eq. (10) in Ref. [26].

The $2\Gamma_\lambda(\omega_\lambda)$ is the phonon linewidth of the phonon mode λ whose inverse is phonon relaxation time [36],

$$\tau_\lambda = \frac{1}{2\Gamma_\lambda(\omega_\lambda)}. \quad (3)$$

Shao *et al.* [27] have already verified that the RTA results negligibly underestimate k_p compared with the iterative solution. So, we focused on the results using the RTA.

III. RESULTS AND DISCUSSION

A. Crystal-structure and lattice properties

Table I shows the calculated equilibrium crystal-structure parameters of the BiCuOQ compounds. The PBEsol exchange potential based on the DFT calculations gives smaller lattice constants compared to the experimental reports [16]. In general, the PBEsol underestimates the lattice parameter, while the Perdew-Burke-Ernzerhof (PBE) functional slightly overestimates it [27]. Our results for BiCuOSe are in good agreement with previous PBEsol results [19]. As the chalcogen atom changes from S to Te, the cross-plane c axis is more elongated than the in-plane a axis. The c/a ratio changes from 2.2 (BiCuOS) to 2.4 (BiCuOTe), which indicates the distance between BiO and CuQ layers are more sensitively changed than the in-plane lattice with the change of atomic size of the chalcogen atom. Table I also lists the Born effective charges and the dielectric constants of BiCuOQ, which are related to the bond character and the optical phonon splitting in the dispersion relation. Our results indicate that the covalent character of the Bi-O bond is much greater than the Cu-Q bond [19]. The trend with the change of chalcogen atom shows that the increase of the atomic number leads to an increase in the covalent bond character of the Bi-O and Cu-Q [37]. The increase in the dielectric constant also indicates low-frequency phonons in the dispersion and is consistent with the presence of heavy atoms in the BiCuOTe crystal.

Based on the optimized crystal structure, we have calculated the elastic properties of the BiCuOQ compounds listed in Table II. We also estimate the bulk (B) and shear (G) moduli using the Hill average of the Voigt and Reuss bounds. The Young modulus (E) is related to B and G [38] as

$$E = \frac{9BG}{3B+G}. \quad (4)$$

The longitudinal (v_L) and transversal (v_T) sound velocities of the tetragonal crystal are

$$\rho v_L^2 = B + \frac{4}{3}G, \quad \rho v_T^2 = G, \quad (5)$$

where ρ is the density. The Debye temperature (T_D) and frequency (ω_D) are

$$\omega_D = v_A(6\pi^2 n)^{1/3}, \quad T_D = \frac{\hbar\omega_D}{k_B}, \quad (6)$$

where v_A is average sound velocity

$$\frac{3}{v_A^3} = \frac{1}{v_L^3} + \frac{2}{v_T^3}. \quad (7)$$

As the chalcogen atomic number increases, the overall stiffness decreases (soft bonding in the compounds). The underestimation of the lattice parameter gives large elastic properties compared with experimental reports [39] and those

TABLE II. Calculated lattice properties of the BiCuOQ compounds: elastic constants C_{ij}, bulk (B), shear (G), and Young (E) moduli (in GPa), longitudinal and transversal sound speed (v_L,v_T in m/s), Debye temperature (T_D in K), and Debye frequency (ω_D in THz). Available experimental results [39] of the BiCuOSe are also listed.

Compound	c_{11}	c_{12}	c_{13}	c_{33}	c_{44}	c_{66}	B	G	E	v_L	v_T	T_D	ω_D
BiCuOS (this work)	173.8	80.1	73.5	116.2	51.0	41.0	99.6	46.2	120.1	4344	2326	310	6.5
BiCuOSe (this work)	158.1	71.2	66.6	102.8	46.8	36.2	89.6	42.1	109.3	4012	2157	280	5.8
BiCuOTe (this work)	143.9	57.2	58.3	98.8	37.8	22.5	80.3	34.7	91.1	3728	1953	244	5.1
BiCuOSe (exp. [39])									76.5	3290	1900	243	
BiCuOSe (PBE, [27])	137.3	57.7	53.5	94.5	23.8	38.9	76.2		79.6	3650	1814		

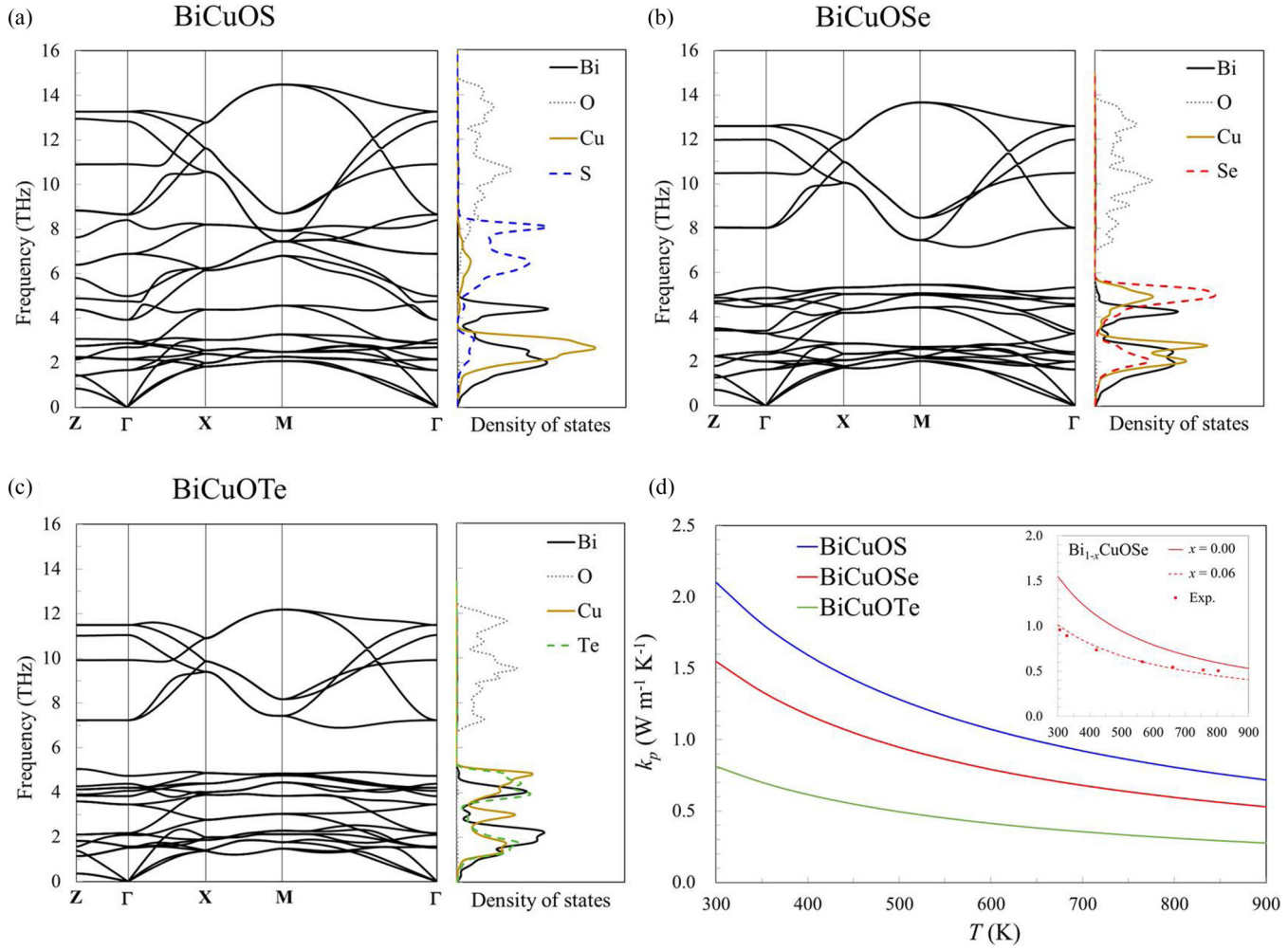

FIG. 2. Phonon dispersions and atomic-projected phonon DOS of (a) BiCuOS, (b) BiCuOSe, and (c) BiCuOTe. (d) Variation of the calculated average phonon conductivity as a function of temperature for BiCuOS (blue), BiCuOSe (red), and BiCuOTe (green). Inset: Comparison between the experimental (Ref. [39], dots) and predicted average phonon conductivity for $Bi_{1-x}CuOSe$ (solid line for $x = 0.00$, dashed line for $x = 0.06$), which is considered a reasonable Bi defect or doping level.

of Shao *et al.* [27], but they are comparable with those of Saha (93 GPa) [19].

B. Phonon dispersion and conductivity

Figures 2(a)–2(c) show the phonon dispersions and atomic-projected density of state (DOS) for each BiCuOQ compound. Based on the lattice properties, the phonon frequencies become lower as the chalcogen atomic number increases, which is also well consistent with the elastic properties. The vibrations of the Bi and O atoms are completely decoupled and the acoustic vibration is mainly from the Bi vibration for all three compounds. For the Cu-Q layer, however, the strength of the coupling of the chalcogen vibration and the Cu vibration increases as the atomic mass increases. In the Cu-S layer, the S vibrational modes are spanning over 5–8 THz and are weakly coupled with the Cu vibrational modes below 3 THz. In the Cu-Se and Cu-Te layers, the chalcogen vibrational modes are redshifted to 2–5 THz and become coupled with the Cu vibrational modes. The overlap of the Cu and chalcogen phonon DOS shown in Fig. 2 indicates that the coupling between the Cu and Q modes becomes stronger as the atomic mass of Q increases. It also indicates that the covalent bonding of the Cu-Q bonds becomes stronger as Q becomes heavier, which is well consistent with the results of the Born effective charge calculation mentioned above. The coupled phonon states of the Cu-Se and the Cu-Te layers show large overlap with the Bi state. Saha [19] discussed that the overlap between the Bi acoustic and the Cu optical (quasiacoustic) vibrations can make for strong acoustic-optical phonon scattering. This is discussed in the next section, with detailed analysis of our phonon-phonon interaction calculations.

The phonon BTE-based k_p results for the BiCuOQ compounds show the expected temperature dependence, evident in Fig. 2(d). Our direction-averaged $k_p = (k_{aa} + k_{bb} + k_{cc})/3$ for the BiCuOSe overestimates the available experimental results, as illustrated in the inset of Fig. 2(d). To verify our predictions, we apply the point-defect phonon scattering model, due to deficiency of Bi atom in the crystal. In BiCuOQ, it has been known that the Bi atom can readily cause defects in the crystal, which in turn induces the phonon scattering. The detailed descriptions of the point-scattering model and

its application are available elsewhere [22,40,41]. Then the experimental results are consistent with the calculation of a Bi defect scattering for $x = 0.06$ [Fig. 2(d), inset].

As the chalcogen atomic number increases, k_p follows the expected trend in the elastic properties (Table II) and phonon dispersions [Figs. 2(a)–2(c)], i.e., the k_p of the BiCuOQ is suppressed as the chalcogen atomic number increases. The extent of suppressions of k_p, however, is much larger than the expectation from the elastic properties, which are closely related with the phonon group velocities. The total mass of the BiCuOSe (734.98 amu) is 1.15 times heavier than that of the BiCuOS (641.19 amu), and BiCuOTe (832.26 amu) is 1.13 times heavier than BiCuOSe.

The square roots of mass differences are also well consistent with the inverse of the ratios of elastic properties and phonon dispersion among BiCuOQ compounds. However, the ratio of k_p between the BiCuOSe and the BiCuOS is 1.35, and even k_p of the BiCuOSe is 1.94 times larger than that of the BiCuOTe. This implies that a simple suppression of phonon frequencies due to mass difference is not the only factor on the k_p suppression.

C. Modal conductivity and phonon linewidth

To investigate the suppression of k_p in the BiCuOQ compounds further, the temperature-dependent modal and accumulated k_p of BiCuOQ compounds are shown in Figs. 3(a)–3(c). To demonstrate more clearly the suppression of k_p for the BiCuOQ compounds, we focus on the in-plane k_p, which is the main contribution to the total k_p. The most

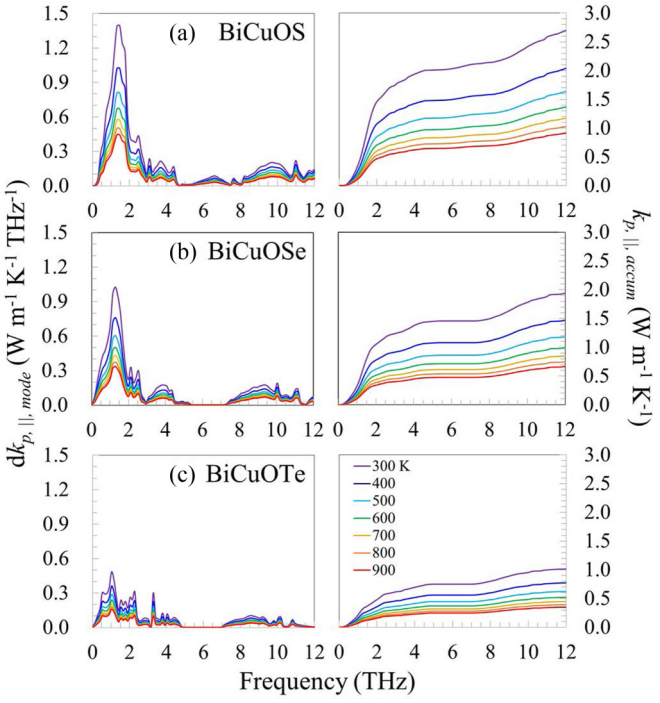

FIG. 3. Frequency dependence of the in-plane modal phonon conductivity (left) and the accumulative phonon conductivity (right) of (a) BiCuOS, (b) BiCuOSe, and (c) BiCuOTe, which corresponds to the area under the modal phonon conductivity. The discrete temperatures are listed in (c).

dominant conductance comes from the acoustic phonon below the 5-THz regime, as indicated in phonon dispersion shown in Figs. 2(a)–2(c). The remaining contribution to k_p is from the high-frequency optical phonon above the 7-THz regime. Similar to other semiconductors, the optical phonon shows a small contribution to k_p and weak temperature dependence. The trend on the chalcogen atom is much more clear in Fig. 3. The modal k_p values of each compound show similar sizes upto 0.5 THz but they show a clear difference above it. The modal k_p peak on the acoustic phonon regime drops around 2 THz for the BiCuOS and BiCuOSe, but the size of the peak around 1 THz is suppressed for the BiCuOSe. For the BiCuOTe, the peak drops rapidly at 1 THz and the overall peak size is much smaller than other compounds. Because the most important differences appear in the acoustic phonon regime, it is crucial to understand why the modal k_p is suppressed in heavy element compounds. In addition to the change of group velocity, we expect that the phonon scattering should be considered as the origin of the rapid drop in the modal k_p in the acoustic phonon regime.

Since the phonon dispersions of these systems are similar and the suppression of dispersion is rather small, as mentioned in the previous section, the effect of phonon scattering is expected to be critical in these systems. So we begin by analyzing the suppression of the modal k_p in detail using the phonon linewidth 2Γ, which is the inverse of relaxation time indicating the scattering strength of the phonon, at 300 K. The low-frequency acoustic phonon regime below 5 THz is illustrated in Figs. 4(a)–4(c). The larger linewidth indicates a larger phonon scattering and shorter phonon relaxation time. The strong scattering occurs at the sudden drop in the modal k_p contribution.

Comparing BiCuOS and BiCuOSe both shows a modal k_p drop at 2 THz, but the BiCuOSe has a larger 2Γ peak near 2 THz compared to the BiCuOS [Figs. 4(a) and 4(b)]. Strong suppression of the modal k_p in the BiCuOTe is clearly seen at 1.5 THz, which is also consistent with the 2Γ peak at the same frequency [Fig. 4(c)].

Note that the distribution of scattering rate (2Γ) is related to the phonon DOS coupling, as mentioned in the description of Fig. 2. Since the scattering is related to the phonon-phonon interaction strength, i.e., Eq. (2), the frequencies at peaks in the scattering rate distribution in Fig. 4 correspond to the peaks in the Cu vibrational mode overlapping with the acoustic Bi vibrational mode [DOS of Fig. 2], which makes the largest contribution to the k_p. As the chalcogen atomic number increases, the vibration of the Cu atom shows strong coupling, which interrupts the Bi vibration and causes the acoustic-optical phonon scattering for these compounds. Comparing the BiCuOS with the BiCuOSe, the Cu vibration is weakly overlapping with the Bi vibration near 2 THz for the BiCuOS, showing a rather small 2Γ. In the BiCuOSe, however, the Cu vibration, which is coupled with the Se vibration, is strongly overlapped with the Bi vibration near the 2- and 5-THz regimes, which is consistent with results presented in Fig. 4(b). Moreover, the heavier chalcogen lowers the peak frequency from 2.5 (BiCuOS) to 1.5 THz (BiCuOTe), as evident in the DOS of Fig. 2 and also indicated by the arrows in Fig. 4. Because the main contribution to k_p is around the 0–2-THz regime, which can be seen as a large area of modal k_p in

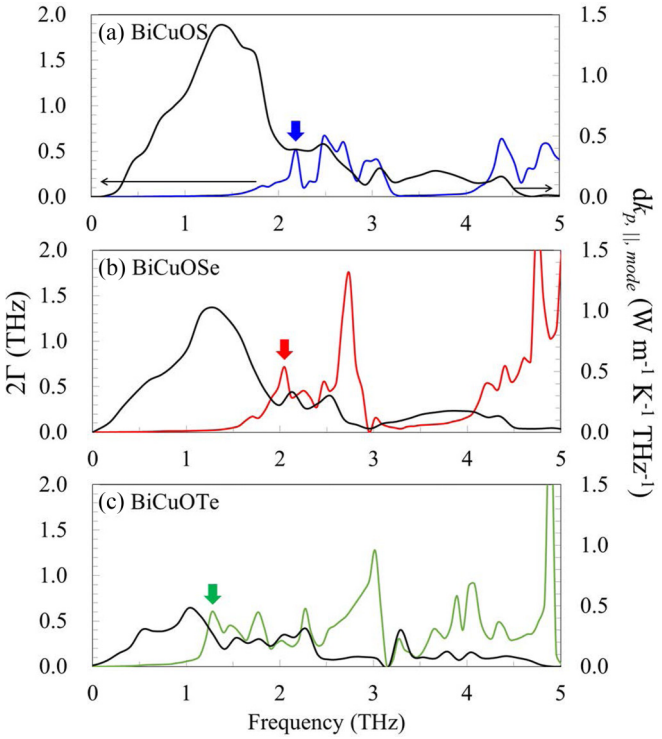

FIG. 4. Calculated modal phonon conductivity (black lines) and phonon linewidth (2Γ, colored lines) at 300 K, in the low-frequency regime, for (a) BiCuOS, (b) BiCuOSe, and (c) BiCuOTe. Colored arrows indicate the frequency of the first phonon linewidth peak, where the modal phonon conductivity is substantially suppressed.

Fig. 4, the first peak in 2Γ is critical in the suppression of total k_p. Note that the Bi and Cu vibrations are contributions from different layers (Fig. 1), so the overlaid independent vibrational modes interrupt each other.

Our result indicates that controlling the elements can control the phonon-phonon interaction and scattering of the phonon by overlapping two independent vibrational states in the layered crystal system. Moreover, this result shows the different layer stacking along the c direction can also affect the in-plane k_p suppression by the interruption of vibrational modes. So, we suggest that the intrinsically heterolayered structure can be a potentially good TE candidate for its electrical properties as well as the phonon scattering. Further studies will verify this interlayer interaction concept by changing the elements in several layered structures both theoretically and experimentally.

IV. CONCLUSIONS

We have investigated the origin of very low phonon conductivity in thermoelectric BiCuOS, BiCuOSe, and BiCuOTe compounds using the first-principles anharmonic, lattice dynamics calculations. The lattice properties and phonon conductivities are predicted considering natural Bi defects in crystals, and our results show good agreement with the reported experiments. To investigate the origin of the low phonon conductivity, the phonon linewidth, which indicates the phonon scattering, was analyzed for these three compounds with different interlayer interactions. We show that the large suppression of phonon conductivity originates from the interaction between vibrations of two independent layers (BiO and CuQ), presented by both the modal phonon conductivity and the phonon lifetime. Strong overlap of the two vibrational frequencies causes strong scattering of the phonon modes, and the BiCuOTe compound offers the smallest phonon conductivity.

We conclude that the mixed-layer structures, including intrinsically heterolayered crystals, are potentially favorable TE material candidates, allowing the engineering of both electronic band gap and phonon thermal conductivity controlled by the interlayer interactions.

ACKNOWLEDGMENTS

This research was supported by Global Frontier Program through the Global Frontier Hybrid Interface Materials (GFHIM) (2013M3A6B1078870), Nano-Material Technology Development Program (2011-0030146), and Basic Science Research Program (2015R1A2A1A15051540, 2015R1D1A1A01059621) through the National Research Foundation of Korea (NRF) funded by the Ministry of Science, ICT & Future Planning/Ministry of Education and by the National Institute of Supercomputing and Network/Korea Institute of Science and Technology Information with supercomputing resources including technical support (KSC-2015-C2-018). M.K. is thankful to the United States NSF program on Thermal Transport and Processes (Award No. CBET1332807).

[1] G. A. Slack, *CRC Handbook of Thermoelectrics* (CRC Press, Boca Raton, FL, 1995).
[2] B. C. Sales, Mater. Res. Soc. Bull. **23**, 15 (1998).
[3] G. J. Snyder, M. Christensen, E. J. Nishibori, T. Caillat, and B. B. Iversen, Nat. Mater. **3**, 458 (2004).
[4] B. Wölfing, C. Kloc, J. Teubner, and E. Bucher, Phys. Rev. Lett. **86**, 4350 (2001).
[5] A. I. Boukai, Y. Bunimovich, J. T.-Kheli, J.-K. Yu, W. A. Goddard, III, and J. R. Heath, Nature (London) **451**, 168 (2008).
[6] R. Venkatasubramanian, E. Siivola, T. Colpitts, and B. O'Quinn, Nature (London) **413**, 597 (2001).
[7] K. F. Hsu, S. Loo, F. Guo, M. W. Chen, J. S. Dyck, C. Uher, T. Hogan, E. K. Polychroniadis, and M. G. Kanatzidis, Science **303**, 818 (2004).
[8] B. Poudel, Q. Hao, Y.Ma, Y. Lan, A. Minnich, B. Yu, X. Yan, D. Wang, A. Muto, D. Vashaee, X. Chen, J. Liu, M. S. Dresselhaus, G. Chen, and Z. F. Ren, Science **320**, 634 (2008).
[9] L. D. Zhao, B. P. Zhang, J. F. Li, M. Zhou, W.-S. Liu, and J. Liu, J. Alloys Compd. **455**, 259 (2008).
[10] L. D. Zhao, S. Lo, J. J. He, H. Li, K. Biswas, J. Androulakis, C. I. Wu, T. P. Hogan, D. Y. Chung, V. P. David, and M. G. Kanatzidis, J. Am. Chem. Soc. **133**, 20476 (2011).

[11] K. Biswas, J. He, I. D. Blum, C. I. Wu, T. P. Hogan, D. N. Seidman, V. P. Dravid, and M. G. Kanatzidis, Nature (London) **489**, 414 (2012).
[12] J. Sui, J. Li, J. He, Y.-L. Pei, D. Berardan, H. Wu, N. Dragoe, W. Cai, and L.-D. Zhao, Energy Environ. Sci. **6**, 2916 (2013).
[13] S. I. Inoue, K. Ueda, H. Hosono, and N. Hamada, Phys. Rev. B **64**, 245211 (2001).
[14] H. Sato, H. Negishi, A. Wada, A. Ino, S. Negishi, C. Hirai, H. Namatame, M. Taniguchi, K. Takase, Y. Takahashi, T. Shimizu, Y. Takano, and K. Sekizawa, Phys. Rev. B **68**, 035112 (2003).
[15] K. Ueda, H. Hiramatsu, H. Ohta, M. Hirano, T. Kamiya, and H. Hosono, Phys. Rev. B **69**, 155305 (2004).
[16] H. Hiramatsu, H. Yanagi, T. Kamiya, K. Ueda, M. Hirano, and H. Hosono, Chem. Mater. **20**, 326 (2008).
[17] C. Lee, J. Hong, M.-H. Whangbo, and J. H. Shim, Chem. Mater. **25**, 3745 (2013).
[18] D. Zou, S. Xie, Y. Liu, J. Lin, and J. Li, J. Mater. Chem. A **1**, 8888 (2013).
[19] S. K. Saha, Phys. Rev. B **92**, 041202(R) (2015).
[20] T.-H. An, Y. S. Lim, H.-S. Choi, W.-S. Seo, C.-H. Park, G.-R. Kim, C. Park, C. H. Lee, and J. H. Shim, J. Mater. Chem. A **2**, 19759 (2014).
[21] B.-L. Huang and M. Kaviany, Phys. Rev. B **77**, 125209 (2008).
[22] H. S. Ji, H. Kim, C. Lee, J.-S. Rhyee, M. H. Kim, M. Kaviany, and J. H. Shim, Phys. Rev. B **87**, 125111 (2013).
[23] H. Kim and M. Kaviany, Phys. Rev. B **86**, 045213 (2012).
[24] H. Kim, M. H. Kim, and M. Kaviany, J. Appl. Phys. **115**, 123510 (2014).
[25] L. Chaput, Phys. Rev. Lett. **110**, 265506 (2013).
[26] A. Togo, L. Chaput, and I. Tanaka, Phys. Rev. B **91**, 094306 (2015).
[27] H. Shao, X. Tan, G.-Q. Liu, J. Jiang, and H. Jiang, Sci. Rep. **6**, 21035 (2016).
[28] P. E. Blöchl, Phys. Rev. B **50**, 17953 (1994).
[29] G. Kresse and D. Joubert, Phys. Rev. B **59**, 1758 (1999).
[30] G. Kresse and J. Furthmüller, Phys. Rev. B **54**, 11169 (1996).
[31] J. P. Perdew, A. Ruzsinszky, G. I. Csonka, O. A. Vydrov, G. E. Scuseria, L. A. Constantin, X. Zhou, and K. Burke, Phys. Rev. Lett. **100**, 136406 (2008).
[32] H. J. Monkhorst and J. D. Pack, Phys. Rev. B **13**, 5188 (1976).
[33] K. Parlinski, Z-. Q. Li, and Y. Kawazoe, Phys. Rev. Lett. **78**, 4063 (1997).
[34] A. Togo, F. Oba, and I. Tanaka, Phys. Rev. B **78**, 134106 (2008).
[35] M. Kaviany, *Heat Transfer Physics*, 2nd ed. (Cambridge University Press, New York, 2014).
[36] A. A. Maradudin and A. E. Fein, Phys. Rev. **128**, 2589 (1962).
[37] In Table I, only the Cu-Te bond has exceptional value in the trends of the Born effective charge. This may be explained by the near zero band gap calculated for the BiCuOTe using the PBEsol potential. Except for the Born effective charge, the other lattice properties of the BiCuOTe follow the trends, so we maintain the consistency by using the exchange potential of the BiCuOQ compounds.
[38] R. Hill, Proc. Soc. A **65**, 349 (1952).
[39] Y.-L. Pei, J. He, J.-F. Li, F. Li, Q. Liu, W. Pan, C. Barreteau, D. Berardan, N. Dragoe, and L.-D. Zhao, NPG Asia Mater. **5**, e47 (2013).
[40] P. G. Klemens, Phys. Rev. **119**, 507 (1960).
[41] J. Callaway and H. C. von Baeyer, Phys. Rev. **120**, 1149 (1960).